ELSEVIER

Physica B 221 (1996) 342–356

PHYSICA B

Neutron scattering studies of magnetic thin films and multilayers

C.F. Majkrzak

Reactor Radiation Division, Materials Science and Engineering Laboratory, National Institute of Standards and Technology, Gaithersburg, MD 20899, USA

Abstract

The basic principles of the elastic scattering of polarized neutrons from magnetic films and thin film superlattices, both kinematically as well as dynamically in the continuum limit, are summarized first. The quantitative accuracy presently attainable in practice is discussed along with other relevant issues regarding experimental technique and data analysis. Investigations of interlayer coupling and the effects of strain and finite thickness in single crystalline, epitaxially grown superlattices are reviewed, focussing on specular neutron diffraction and reflectivity measurements. These superlattices include rare earth and semiconductor systems in addition to those that exhibit "giant" magnetoresistive effects and which are of particular current technological interest. A survey of some of the more recent studies of the enhancement/reduction of ferromagnetic moments at an interface with a nonmagnetic material is then presented. Finally, several future research directions, for example, magnetic nonspecular scattering and studies of the magnetic state of the materials which form the intervening layers between coherently coupled ferromagnetic layers in superlattices, are discussed.

1. Introduction

Historically, neutron scattering has proved to be the definitive method for determining both the microscopic magnetic structure and dynamics in bulk materials [1]. It has been demonstrated in more recent times that elastic neutron scattering can also be used to ascertain the magnitudes and orientations of ordered configurations of atomic magnetic moments in thin films and multilayers. Unlike other important surface-sensitive magnetic probes, such as MOKE (magneto-optic kerr effect), which gives an averaged magnetization over the entire sample film thickness, or SEMPA (scanning electron microscopy with polarization analysis), which shows the domain magnetization direction at the surface of a material in vacuum, elastic specular neutron scattering yields the microscopic in-plane vector magnetization depth profile. Neutron scattering is particularly sensitive to the magnetic state of a material when the incident beam is polarized and analysis of the polarization state of the scattered beam is performed.

The purpose of this paper is to show what has been and can be learned about the effects of lattice strain, finite size, and interlayer coupling on the magnetic structure of thin films or multilayers from the scattering of polarized neutrons. Some of the important experiments which illustrate the power and uniqueness of polarized neutron scattering are reviewed, although the review is by no means meant to be comprehensive. The discussion of experimental results is restricted primarily to single crystalline films and superlattices because of the ability to more directly control and interpret the effects of crystallographic orientation and epitaxial strain. Before presenting specific examples, however, a summary of the experimental methodology and theoretical analysis of polarized neutron scattering from thin films and multilayers is given.

2. Theoretical outline

In this section the essential theory describing the scattering of polarized neutrons by spin-dependent magnetic

SSDI 0921-4526(95)00948-5

potentials is summarized. One of the greatest advantages of neutron scattering is that the interaction of the neutron with the nucleus and atomic magnetic moment is relatively simple, being described by scattering lengths. The coherent nuclear scattering length, b, is in effect a single scalar quantity if we assume a random or disordered population of nuclear spin orientations. The coherent magnetic scattering length, p, is proportional to the magnitude of the atomic magnetic moment but is also dependent on the scattering angle. The coherent scattering of neutrons by a collection of ordered magnetic moments also depends upon the relative orientations of the neutron polarization vector, the atomic magnetic moment, and the wave vector transfer. A detailed description of these fundamental interactions is given in Ref. [1]. Because of the vectorial nature of the magnetic interaction, it is possible to obtain, in addition to its magnitude, the orientation of the atomic magnetic moment from polarized neutron scattering (PNS) data.

In Fig. 1 is shown a typical geometry for the specular elastic scattering of polarized neutrons from a series of atomic reflecting planes, some of which are magnetic. Over the lateral coherence length of the incident neutron plane wave, the individual in-plane atomic moment directions which contribute to a coherently reflected plane wave are effectively averaged. The neutron polarization is, in this particular case, taken to be along the vertical axis, either spin "up" or "down", perpendicular to the wave vector transfer Q. Any out-of-plane component of the magnetization does not contribute to the scattering. In this particular geometry, a projection of a given atomic plane's magnetization onto the vertical axis gives rise to non-spin-flip (NSF) scattering of the neutron (which interferes with the nuclear scattering) whereas a projection onto the horizontal axis creates spin-flip (SF) scattering (which does not interfere with the nuclear scattering), as can be determined from the formulas in Table 1. The values of the coherent scattering lengths are assumed to be averaged over either an individual atomic plane or volume of a layer of prescribed thickness, as the case may be.

Spin-dependent reflectivities (ratio of reflected to incident intensity) corresponding to NSF (++ and −−) and SF (+− and −+) processes can be measured as a function of angle of incidence or wave vector transfer Q (as will be demonstrated in Section 3). From such data the vector magnetization depth profile can be reconstructed using the formulas summarized in Table 1. It is convenient to separate the range of wave vector transfer into two parts, one at low Q (and relatively high reflectivity), where the scattering medium can be treated as a continuum, and the other at high Q (and relatively low reflectivity), where the discrete nature of the atomic planes becomes manifest. In the low-Q regime, it is often necessary to use an exact or dynamical formula for the scattering which takes into account significant distortions of the incident plane wave during interaction

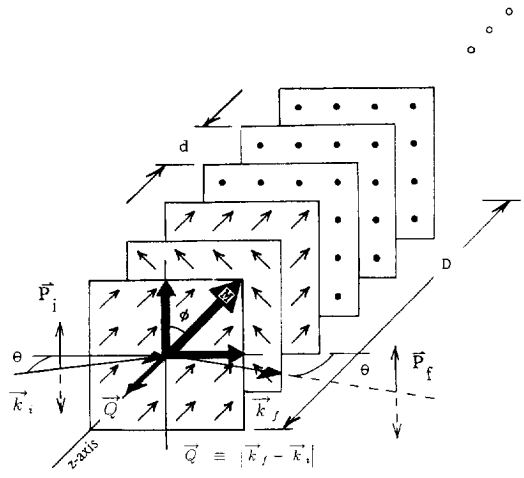

Fig. 1. Elastic specular scattering geometry for a single crystalline superlattice. P is the neutron polarization vector, k the neutron wave vector, and Q the wave vector transfer (the subscripts i and f refer to incident and final states, respectively). The distances d, D, and L correspond to interatomic plane spacing, chemical bilayer thickness, and total superlattice thickness, respectively. M is the net in-plane magnetization of an atomic plane and is proportional to the magnetic scattering length p.

with the scattering medium. At sufficiently high values of Q the Born approximation is valid (negligible distortion of the incident plane wave). We will adopt a somewhat arbitrary convention and refer to PNS as polarized neutron reflectivity (PNR) in the low-Q regime and as polarized neutron diffraction (PND) at high-Q.

A detailed description of PNS in the kinematic limit and where only the initial and final spin eigenstates of the neutron are determined (in contrast to the neutron polarization vectors) was given by Blume [2] and by Moon et al. [3]. A thorough description is also given in Bacon [1]. For those magnetic structures which rotate the neutron polarization vector out of alignment with the quantization axis, it is useful to perform three-dimensional polarization analysis, as first done by Rekveldt [4] and advanced by Okorokov [5], Tasset et al. [6], and Nunez et al. [7], who utilized a zero-field sample environment.

Although there have been some more recent discussions [8, 9], the dynamical theory of polarized neutron scattering from magnetic materials was fully developed many years earlier by Mendiratta and Blume [10], Sivardiere [11], and Belyakov and Bokun [12], among others. Scharpf [13] extended the dynamical theory to the continuum limit while Felcher et al. [14], Majkrzak [15], and Majkrzak and Berk [16] made specific application of the dynamical theory to polarized neutron reflectivity from magnetic films and multilayers. The dynamical regime is particularly interesting in regard to the nonclassical effects on the neutron polarization as it tunnels through a magnetic thin film barrier. It

Table 1
Reflectivity formulas ($\rho_s \equiv$ (effective scattering length) (# atoms/unit area), $\rho_v \equiv$ (effective scattering length) (# atoms/unit volume))

Exact (dynamical), high reflectivity, low Q	Born approximation (kinematical), low reflectivity, high Q
$\|R\|^2 = \left\| \frac{4\pi}{Q} \int_0^L \Psi(Q,z)\rho_v(z)e^{i(Q/2)z}\,dz \right\|^2$ (continuum)	$\|R\|^2 \cong \left\| \frac{4\pi}{Q} \int_0^L \rho_v(z)e^{iQz}\,dz \right\|^2$ (continuum)
	$\|R\|^2 \cong \left\| \frac{4\pi}{Q} \sum_{j=0}^{N-1} \rho_{sj}(z_j)e^{iQz_j} \right\|^2$ (discrete atomic planes)

To obtain $|R|^2$, solve the corresponding pair of coupled wave equations for ψ_+ and ψ_- ($\Psi = \psi_+ + \psi_-$ in case of polarized beams) in piecewise continuous fashion by imposing continuity of wave functions and their first derivatives at each boundary in a layered representation of the scattering medium. In each layer the scattering length density (scalar nuclear component and vecotor magnetic part) is taken to be constant. Each layer or slab can be characterized by a 4×4 matrix $\boldsymbol{A}_j$. The spin-dependent reflectivities $|R|^2$, transmissions $|T|^2$, and incident beam (of polarization defined by I_+ and I_-) are then related by

$$\begin{pmatrix} T_- \\ T_- \\ \frac{iQ}{2}T_+ \\ \frac{iQ}{2}T_- \end{pmatrix} = \prod_{j=N}^{1} \boldsymbol{A}_j \begin{pmatrix} I_+ + R_+ \\ I_- + R_- \\ \frac{iQ}{2}[I_+ - R_+] \\ \frac{iQ}{2}[I_- - R_-] \end{pmatrix}$$

Note: (a) Substrates should be included in above matrix equation if present; and (b) the component of $\boldsymbol{B}$ or $\boldsymbol{M}$ perpendicular to the interface must be continuous as required by Maxwell's equations. Thus, only in-plane components of $\boldsymbol{B}$ result in specular scattering.

Consider the particularly useful geometry where the neutron polarization axis and sample magnetizations are perpendicular to $\boldsymbol{Q}$: the effective coherent spin-dependent scatterings lengths in this configuration are:

$b_j + p_j \cos\phi_j$ (for $|R_{++}|^2$),

$b_j - p_j \cos\phi_j$ (for $|R_{--}|^2$) and

$p_j \sin\phi_j$ (for $|R_{+-}|^2$ and $|R_{-+}|^2$),

where b_j is a nuclear scattering length and p_j is proportional to $\boldsymbol{M}_j$ (scattering angle dependence of p_j is implicit).

Note: (a) For a periodic superlattice, the sum over all N atomic planes can be replaced with a sum over a single unit cell multiplied by the factor $\sin(MQD/2)/\sin(QD/2)$ where M is the number of unit cells and D is the thickness of a cell; and (b) Debye–Waller factors which take into account the effects of thermal vibrations have not been included.

was shown by Buttiker [17] that in tunnelling through such a barrier, both a precession about as well as a rotation towards the magnetic field axis occurs and that the angle of precession is independent of the barrier width. These dynamical polarization effects have been analyzed in more detail by Nunez et al. [18] and three-dimensional polarization analyzes of neutrons transmitted through (as well as those reflected by) an iron thin film barrier, with a remanent magnetization in zero applied field, have been performed which confirm some of Buttiker's predictions [19, 20]. Bland et al. [21] have even proposed measuring the rotation of the neutron's polarization as an alternative means (to conventional PNR measurements) of inferring the magnetic moment per atom in an epitaxial film.

Another useful configuration, for investigating helical magnetic structures, for instance, is to arrange it so that the neutron polarization axis is parallel to Q (which is perpendicular to the reflecting atomic planes in which the magnetization, or at least some rotating component of which, lies). In this case right- and left-handed spirals have different spin-dependent reflectivities and can, consequently, be distinguished. For more detailed discussions of the scattering of polarized neutrons from superlattices, Refs. [22, 23] can, for example, be consulted. However, in summary, using either the dynamical or kinematic theories, the reflectivity for a model magnetic structure can be calculated straightforwardly, including the effects of strain and compositional variations (e.g., interdiffusion), for comparison with PNS data. Furthermore, given the chemical structure from independent X-ray scattering measurements, the magnetic structure can be solved for directly, with sufficient neutron data, at least in the kinematic limit.

3. Experimental methods

A schematic representation of an experimental configuration for carrying out PNR or PND is pictured in Fig. 2. A monochromatic neutron beam can be efficiently polarized by a magnetic supermirror of the type first proposed by Mezei [24] which makes use of the interference between nuclear and magnetic scattering from a magnetic

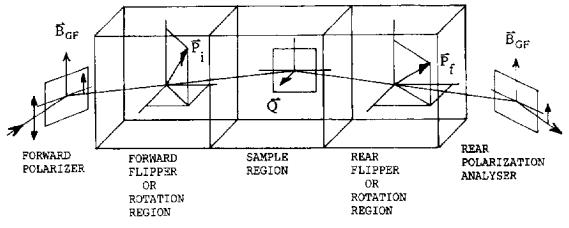

Fig. 2. Schematic representation of experimental setup for selecting polarization of incident neutron beam and analyzing polarization of beam scattered by sample as described in the text.

multilayered thin film structure to reflect predominantly only one spin state with respect to a fixed magnetic guide field or quantization axis. The use of a series of separate but adjacent magnetic field regions with well-defined, sharp boundaries (across which the neutron polarization vector P makes a sudden transition) makes it possible to select the initial and analyze the final neutron polarization vectors. Within the regions preceding and following the sample, an applied magnetic field can be defined in any direction by appropriate contributions from three mutually orthogonal components as supplied, for example, by three intersecting, perpendicular, rectangular solenoidal wire coils: the neutron polarization can then be made to precess adiabatically to any desired orientation prior to entering the adjacent field region. This method for rotating the neutron polarization was introduced by Rekveldt [25]. In practice, particularly in the polarimetry work cited in the preceding section, Meisner shields are used to create the sharp boundaries needed between adjacent magnetic field regions.

If the sample is an antiferromagnet, whether collinear or not, the net magnetization is zero and no field need be applied in the sample region. Nor does a field need to be applied if the sample is a remanent single domain ferromagnet (assuming that the return fields of the ferromagnetic sample cause negligible precession of the neutron polarization in this region). Any direction of the incident neutron polarization can be chosen using the rotation field region preceding the sample area. Samples with certain magnetic structures can cause a rotation of the neutron polarization vector other than flipping from one eigenstate to the other. In any event, the final neutron polarization direction can be analyzed by using the rotation field region following the sample to project out, one at a time, the rectangular components of the final polarization vector onto the quantization axis or guide field direction of the polarization analyzer. Of course, a magnetic field can be applied at the sample position with the incident and reflected neutron polarization axes parallel to it if only SF and NSF reflectivities are to be measured.

If, on the other hand, the sample is a multidomain ferro- or ferrimagnet, then a saturating magnetic field must be applied to avoid neutron depolarization (unless that is what is to be measured!). In this case the neutron polarization axis should be along this applied field with the neutron polarization either parallel or antiparallel (so that, again, only initial and final eigenstates of the neutron are measured).

The supermirror polarizers which are presently available have high reflectivities ($\sim 95\%$), high polarizing efficiency ($\sim 95\%$), and are well-matched to the angular beam divergences and wavelength spreads typically required for neutron scattering (a few minutes of arc and several percent, respectively), at least at longer neutron wavelengths ($\sim > 2$Å) [26, 27]. Flipping efficiencies of the type of flipper described above are also good ($\sim 99\%$). Nevertheless, the polarizing and flipping efficiencies are not perfect and appropriate instrumental corrections need to be made for accurate quantitative measurements. In Table 2 is outlined a procedure which can be used to make the requisite corrections. Any beam depolarization which occurs in the guide field is implicitly included as part of the effective polarizing element, depending on where the depolarization occurs, i.e., prior to or following the sample. The four spin-dependent reflectivities can be determined from the measured scattered intensities for the four possible combinations of front and rear flipper states if the front and rear polarizer and flipper efficiencies can be determined using an appropriate reference sample.

As an example of the corrections described above and their implementation, consider the uncorrected reflectivity data for a (0 0 1) [Fe(38 ml)/Cr(8 ml)]×5 (ml = monolayers or atomic planes) superlattice plotted in Fig. 3 [29]. The presence of ferromagnetic Fe is clearly evident by the appearance of two distinct critical cutoffs for total external mirror reflection near $Q = 0.02$ and in the greatly different

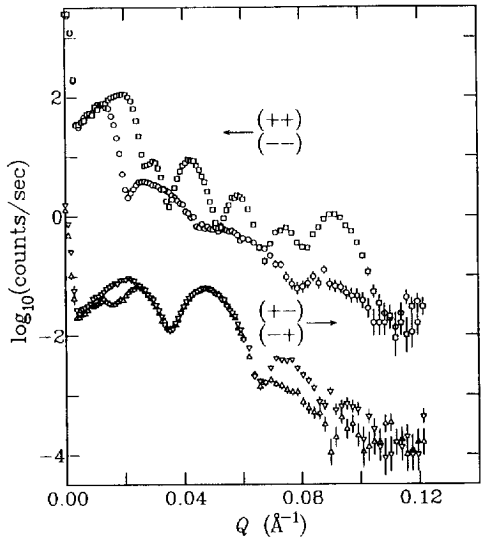

Fig. 3. Uncorrected polarized neutron reflectivity data for a (0 0 1) [Fe(38 ml)/Cr(8 ml)]×5 superlattice. Note the difference in (+−) and (−+) intensities located about a Q of 0.02.

Table 2
Polarizing and flipping efficiency corrections

The relationship between the intensities measured in the detector and the sample spin-dependent reflectivities [28] are

$$I^{\text{off off}}/\beta = \sigma_{++}(1+F)(1+R) + \sigma_{-+}(1-F)(1+R) + \sigma_{--}(1-F)(1-R) + \sigma_{+-}(1+F)(1-R),$$

$$I^{\text{on off}}/\beta = \sigma_{++}(1+R)[1+F(1-2f)] + \sigma_{-+}(1+R)[1-F(1-2f)] + \sigma_{--}(1-R)[1-F(1-2f)] + \sigma_{+-}(1-R)[1+F(1-2f)],$$

$$I^{\text{off on}}/\beta = \sigma_{++}(1+F)[1+R(1-2r)] + \sigma_{-+}(1-F)[1+R(1-2r)] + \sigma_{--}(1-F)[1-R(1-2r)] + \sigma_{+-}(1+F)[1-R(1-2r)],$$

$$I^{\text{on on}}/\beta = \sigma_{++}[1+F(1-2f)][1+R(1-2r)] + \sigma_{-+}[1-F(1-2f)][1+R(1-2r)] + \sigma_{--}[1-F(1-2f)][1-R(1-2r)] + \sigma_{+-}[1+F(1-2f)][1-R(1-2r)].$$

The spin-dependent reflectivities can be solved for from the measured intensities if the instrumental polarizing and flipping efficiencies and the constant β are determined.

The constant β is given by

$$2\beta = \frac{I_{\text{NS}}^{\text{on on}} I_{\text{NS}}^{\text{off off}} - I_{\text{NS}}^{\text{on off}} I_{\text{NS}}^{\text{off on}}}{I_{\text{NS}}^{\text{on on}} + I_{\text{NS}}^{\text{off off}} - I_{\text{NS}}^{\text{on off}} - I_{\text{NS}}^{\text{off on}}} \equiv \alpha$$

where the subscript "NS" signifies measurements at zero scattering angle with "no sample" in place. Also,

$$I_{\text{NS}}^{\text{off off}}/\alpha = FR + 1,$$

$$I_{\text{NS}}^{\text{on off}}/\alpha = FR(1-2f) + 1,$$

$$I_{\text{NS}}^{\text{off on}}/\alpha = FR(1-2r) + 1,$$

so that f, r, and the product FR can be determined.

If the sample is replaced with a "reference sample" (RS) which has $\sigma_{+-} \neq \sigma_{--}$ and $\sigma_{+-} = \sigma_{-+} = 0$ (σ_{++} and σ_{--} need not be known), then F and R can be individually determined.

σ_{++}, σ_{--}, σ_{+-}, and σ_{-+} are defined as the NSF and SF reflectivities, respectively, corresponding to the sample.
$I^{\text{off off}}$, $I^{\text{on on}}$, $I^{\text{off on}}$ and $I^{\text{on off}}$ are defined as the intensities measured with front and rear flippers, respectively, in "on" (π rotation of the neutron spin) or "off" (no rotation) states.
F, R, f, and r are defined as the front and rear polarizer and front and rear flipper efficiencies, respectively.

intensities of the NSF scattering for the primary multilayer diffraction peak at a Q of approximately 0.09 Å^{-1}. These reflectivity curves also indicate, incidentally, that the magnetic and chemical structures are coherent over the entire thickness of the multilayer. Correcting for refractive shifts, a pronounced peak appears in the SF reflectivity data at a Q corresponding to a doubling of the fundamental chemical bilayer period. Since in this configuration the SF scattering is purely magnetic in origin, it can be immediately inferred that the magnetic unit cell is twice that of the chemical spacing and that successive ferromagnetic Fe slabs have relative moment orientations which are not parallel. (The Fe layers or slabs are oriented in a noncollinear arrangement in this sample.) Fig. 4 shows the result of correcting the raw data for background, beam footprint, and instrumental polarizing and spin flipping efficiencies. Note especially that the difference in the +− and −+ SF reflectivities in the region about $Q = 0.02$ for the raw data of Fig. 3 is an instrumental artifact arising from the nonperfect front and rear polarizer and flipper efficiencies and is absent in the corrected data of Fig. 4.

Fig. 5 shows corrected neutron reflectivity data for a different (0 0 1) [Fe(38 ml)/Cr(6 ml)]×5 superlattice along with a quantitative nonlinear least-squares fit (solid line) using the dynamical theory outlined in Table 1 [29]. The corresponding nuclear and magnetic scattering length density profiles and Fe layer magnetization directions are plotted in Fig. 6 and reveal a simple antiferromagnetic alignment of the Fe blocks in this specimen. This is a good example of how PNR can give, both qualitatively and quantitatively, an accurate picture of the microscopic magnetic structure of such superlattice structures. What is also remarkable is that these data were obtained from a sample with a film surface area less than a square cm and with a volume of only a few millionths of a cubic cm. With larger surface areas, it has in fact been possible to measure reflectivities as low as 10^{-7}.

Before concluding this section, it should be mentioned that for specular reflectivity measurements of the kind discussed above, it is important that the sample area be macroscopically flat on the order of the instrumental resolution. That is, in an angular scan about a sample axis of rotation

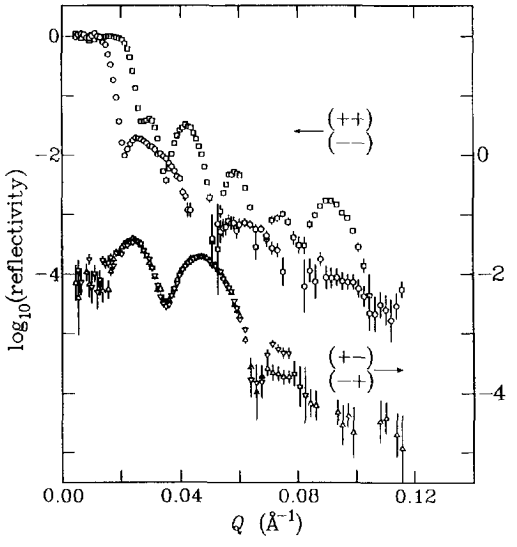

Fig. 4. Polarized neutron reflectivities for the same Fe/Cr superlattice of Fig. 3 after correction for geometrical factors and instrumental polarizing and flipping efficiencies. Note that the discrepancy between the two SF intensities which appeared in Fig. 3 about a Q of 0.02 has vanished. (After Ref. [29].)

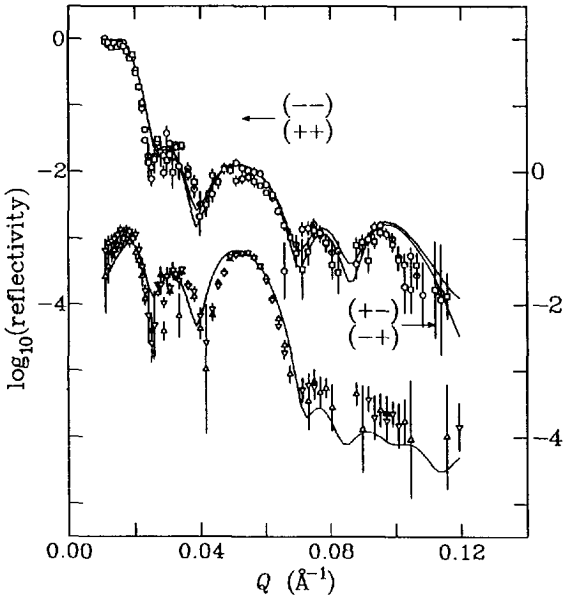

Fig. 5. Polarized neutron reflectivity data (symbols) for a different (0 0 1) [Fe(38 ml)/Cr(6 ml)]×5 superlattice with simple antiparallel alignment of the Fe layers. The solid line curves are fits obtained for the scattering length density profiles and magnetization orientations plotted in Fig. 6 and using the dynamical theory outlined in Table 1. (After Ref. [29].)

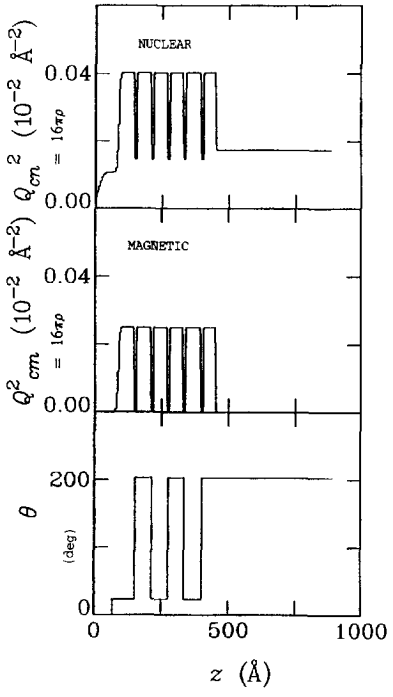

Fig. 6. Scattering length density profiles and relative orientation angles of the Fe layer magnetizations corresponding to the calculated reflectivities for the Fe/Cr superlattice shown in Fig. 5. (After Ref. [29].)

which is perpendicular to the plane of reflection defined by incident and final neutron wave vectors, and with the detector at a fixed scattering angle, the angular width of the specular intensity in this so-called "rocking curve" should be of the order of the instrumental angular divergence, typically a minute of arc. If the angular width of the specular component is found to be larger than the incident beam divergence due to a deviation of the sample from perfect flatness, than the angular acceptance of the analyzer and detector must be sufficiently open to accept the entire specular contribution. Furthermore, in the analysis of the specular scattering described above, it is assumed that the nonspecular or diffuse scattering arising from in-plane interfacial roughness is sufficiently small that it constitutes a negligible perturbation. References to the treatment of nonspecular scattering are cited in some of the discussions of experiments below.

4. Research review

In the following subsections, some of the PNS work which has been done on epitaxial thin films and superlattices is discussed. As mentioned in Section 1, the review is not intended to be exhaustive. Instead, a number of studies have been selected which illustrate how the use of PNS in

determining magnetic microstructures can lead to a better understanding of fundamental magnetic interactions.

4.1. Rare earth superlattices

Long-range indirect exchange, crystal field anisotropy, and magnetostrictive effects are characteristic properties of the magnetic rare earth (RE) elements. In the 1980s it was learned how to grow RE single-crystalline thin films and superlattices in ultrahigh vacuum by molecular beam epitaxy with atomic-plane precision and with limited interdiffusion across dissimilar material interfaces [30, 31]. It consequently became possible to create magnetic layers thin enough to exhibit effects of reduced dimensionality, introduce lattice strain at the interface with another material, and to separate successive magnetic layers (each consisting of a certain number of atomic planes) by an intervening nonmagnetic spacer of arbitrary thickness. Systematic PNS studies of the results of such atomic-scale chemical engineering on the magnetic ordering have subsequently been performed. Some of the important findings of these studies are discussed below. More comprehensive reviews of the earlier PNS work on magnetic RE superlattices are given in Refs. [22, 32].

4.1.1. Gd/Y

The first coherent, long-range, antiparallel coupling of ferromagnetic layers across intervening nonmagnetic layers was discovered by PNS to occur in Gd/Y superlattices [33]. For certain thicknesses of the Y layer, the coupling between successive Gd layers was parallel whereas for others it was antiparallel. It was found that these two relative orientations of the Gd layer magnetizations had, in fact, an oscillatory dependence on the Dy layer thickness in a manner consistent with a simple RKKY indirect exchange model of the interlayer coupling mechanism [34]. Fig. 7 shows how the antiparallel coupling could be conclusively identified using PND by the appearance of predominantly SF scattering at superlattice satellite positions corresponding to a period double that of the chemical bilayer. In Fig. 8 is a schematic representation of the antiparallel configuration (slighty canted by the presence of an applied field) for a [Gd(10 ml)/Y(10 ml)]×225 superlattice. The inset shows the relative sign and strength of the coupling between adjacent Gd layers across the intervening Y as predicted by the RKKY interaction model [33, 34].

Given the detailed lattice strain and compositional profiles obtained from X-ray diffraction measurements [35], it was also possible to obtain by PND the magnetization of each of the 10 (nominally) (0 0 2) basal planes composing a Gd layer in a Gd/Y superlattice with parallel alignment [36]. The moment per atom was found to be about 5.7 Bohr magnetons for the interior planes, but decreased to zero across an interfacial width of approximately 3 atomic planes.

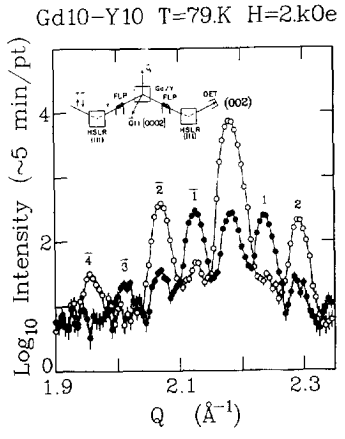

Fig. 7. NSF (open circles) and SF (filled circles) scattering from a [Gd (10 ml)/Y(10 ml)]×225 superlattice (the data shown here are not corrected for instrumental polarizing and flipping efficiencies). The SF scattering which appears at values of Q corresponding to a doubling of the chemical bilayer spacing (odd-numbered satellites) is consistent with an antiparallel alignment (as the applied field approaches zero) of successive ferromagnetic Gd layers as depicted schematically in Fig. 8. (After Ref. [33].)

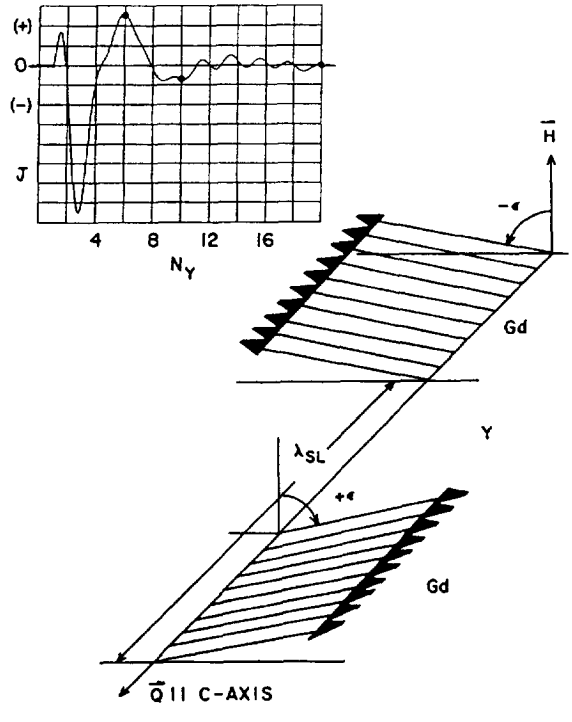

Fig. 8. Real space schematic of the Gd/Y superlattice of Fig. 7. The inset shows the relative strength and sign of the coupling between adjacent Gd layers across the intervening Y as predicted by an RKKY interaction model. (After Ref. [33].)

4.1.2. Dy/Y

Bulk Dy orders magnetically as an incommensurate basal plane spiral with a helical turn angle between adjacent ferromagnetic (0 0 2) atomic planes that varies with temperature. At lower temperatures, a first-order transition to a simple ferromagnetic state occurs, driven by magnetostriction. Neutron diffraction studies of Dy/Y superlattices first performed by Rhyne et al. showed that, up to a certain Y layer thickness, both the chirality and phase of the Dy spirals are preserved across the Y spacers [37], the coherence of the Dy spiral extending over many chemical bilayer periods (as evident from the nearly resolution-limited widths of the spiral satellite reflections). Flynn et al. [40] investigated Dy/Y superlattices grown with the chemical modulation along the *b*-axis rather than the HCP *c*-axis. In this case the Dy spiral was found to be coherent only across the thickness of an individual Dy slab (the chemical structure was still coherent over many bilayer repeats). This result was predicted from calculations of the strength of the interaction along the two different crystallographic directions: the interaction strength decreases about an order of magnitude faster along the *b*-axis compared to the *c*-axis where the effective range is approximately 100 Å. An extension of the simple RKKY theory used to explain the interlayer coupling in the Gd/Y superlattices was formulated by Yafet [38] to correctly predict some of the observed behavior of the Dy/Y system, namely the chiral coherency and order of magnitude of the interlayer coupling strength, in which a helical RKKY field is set up in the Y. Nonetheless, the actual polarization of the conduction electrons in the Y metal spacer is not yet certain. The interlayer coupling in magnetic RE superlattices is discussed in more depth in Ref. [32] and in a review by Yafet [39] which focusses on interlayer magnetic coupling in both localized and itinerant magnet superlattices.

4.1.3. Dy/Lu

In the *c*-axis Dy/Y superlattices discussed above, it was also found that the first-order transition to a ferromagnetic state which occurs in bulk Dy is suppressed to lower and lower temperatures as the thickness of the Dy layer is decreased. This effect has been attributed to the relatively large mismatch between basal plane lattice constants for Dy and Y (~1.6%). The *a*- and *b*-axis lattice parameters of Dy are significantly expanded, while its *c*-axis lattice parameter is contracted, when epitaxially grown on a basal plane of Y. Thus, the magnetostriction across the Dy layer is modified from that of bulk Dy, consequently affecting the transition to the ferromagnetic phase which depends on the appropriate change in magnetoelastic energy [41]. In contrast, in Dy/Lu superlattices the epitaxial growth of Dy on Lu results in a compression of the Dy basal plane lattice parameters with the result that the transition to a ferromagnetic state is enhanced (although a quantitative understanding in terms of the magnetoelastic energy is not as straightforward as in the case of Dy/Y) [42]. Fig. 9 shows the difference in the neutron diffraction data for spiral and ferromagnetic Dy layer states (note that the ferromagnetic Dy layers are themselves in antiparallel alignment with one another) [42]. For a detailed discussion of the role the magnetoelastic energy plays in determining the magnetic structure of rare earth superlattices and films, see Rhyne and Erwin [32].

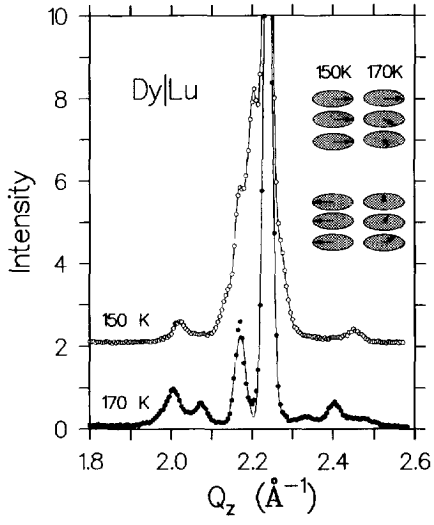

Fig. 9. Neutron diffraction scans for a [Dy(21 ml)/Lu(10 ml)] superlattice show that below 160 K the helical order of the Dy layers is transformed into ferromagnetic blocks which are aligned antiparallel to one another. The satellite peak widths demonstrate that the helimagnetic state is of shorter range than the ferromagnetic state: note also that there is apparently some remanence of the helix in the ferromagnetic phase. (After Ref. [42].)

4.1.4. Ho/Y

Bulk Ho has a relatively complicated spiral magnetic structure in which the in-plane magnetizations of the ferromagnetic basal planes are incrementally rotated from one another along the *c*-axis, but not exactly uniformly. The spiral is distorted by a bunching of the moments along the six-fold easy directions defined by the HCP basal plane crystal field. A unified picture of this distorted structure has been developed in which the bunching is described by sequences of "spin-slips" [43–46].

Bohr et al. [47] have argued that the magnetic moment arrangement inside a given block of Ho planes in a Ho/Y superlattice might be primarily determined by the interplanar interactions within that block alone, allowing for the effect of the strain introduced by the artificial layering. A turn angle profile sufficiently detailed to allow definite conclusions to be drawn regarding the possible influence of finite size was not obtained, however.

More recent work on Ho/Y superlattices has been reported by McMorrow et al. [48, 49], Jehan et al. [50] and

Cowley et al. [51]. The primary goal of this work was to study more completely the interlayer coupling between Ho layers across the Y as well as the magnetic structure of the Ho spiral within a given block. By quantitatively fitting neutron diffraction profiles for the primary and higher-order satellites arising from the distorted magnetic spiral to model structures, several important results emerged. The best fits were consistent with the absence of any moment on the Y planes and a net turn angle across an intervening Y block which was independent of both temperature and superlattice period. Furthermore, although there is coherence of the chirality and average turn angle of the Ho moments over at least five chemical bilayers, information pertaining to the positions of spin-slips in a given Ho block is apparently not transmitted across the Y layers. This latter finding was deduced from the observation of a fifth-order diffraction harmonic, which is indicative of a distorted spiral or spin-slip structure, whose width implied coherence over only a single Ho layer thickness and also lacked the fine structure of the primary satellite.

4.1.5. *Ho/Er*

The effect of competing crystal-field anisotropies on the magnetic ordering in Ho/Er superlattices was studied using neutron diffraction by Simpson et al. [52]. Within a certain temperature range, the Ho moments are confined predominantly to the basal plane whereas the Er is aligned primarily along the c-axis of the HCP crystal structure. The resulting magnetic structures deduced from the neutron diffraction data are relatively complicated and will not be described in detail here. One of the more striking results, however, is the observed lack of coherence of the c-axis components of the Er moments in the Ho/Er superlattices across the Ho blocks, especially in view of the fact that long-range order has been observed in Er/Y superlattices [53]. Simpson et al. make a convincing argument that their results, in addition to other inconsistencies in the behavior of various RE superlattices, cannot be understood in terms of the conventional RKKY theory used thus far to explain interlayer coupling in the RE superlattices, but require modifications which explicitly allow for the band structure of the superlattice itself. It is a good example of how the microscopic information obtained by neutron diffraction can progressively lead to a more complete and accurate understanding of the intricate coupling mechanisms at work.

4.1.6. *Tb single crystals*

The critical scattering of neutrons in Tb above its magnetic spiral phase transition temperature exhibits a two-component line shape [54–56], as has also been documented in Ho [57], implying the existence of a second length scale. The neutron scattering studies on Tb single crystals cited above established that the scattering associated with this second length scale is strongly enhanced over a few hundred micron thick region near the surface of the crystal but is not evident in the bulk interior. (The transverse Q resolution through the position of the magnetic spiral satellite about the forward direction was 0.00006 Å^{-1} FWHM whereas the spatial width of the beam was 100 μm FWHM!) This intriguing, and possibly surface-related effect, is discussed by Gehring at this Conference [58].

4.2. *Giant magnetoresistance superlattices*

In the ongoing search for improved magnetic storage devices, considerable efforts have been devoted to the fabrication and characterization of magnetic multilayers which exhibit a "giant" magnetoresistance (GMR) [59]. It is believed that the observed increase in electrical resistivity in GMR multilayers such as Co/Cu or Fe/Cr is correlated with an antiparallel alignment of the ferromagnetic Co or Fe blocks: if a sufficiently large external magnetic field is applied to align all of the layer magnetizations in a single direction, then resistance to the transport of electrons diminishes, attributed to a resultant reduction in potential sources of electron scattering. Neutron scattering measurements are ideally suited to help establish this correlation. The GMR effect is observed in both single crystalline superlattices as well as in more disordered multilayers. Indeed, the degree of disorder and crystallographic orientation at the interfaces between the two different material layers can have a significant impact on the magnetoresistive behavior. Numerous neutron reflectivity studies have been performed on Co/Cu and Fe/Cr multilayers and superlattices to obtain evidence of antiparallel alignment [60–67].

To determine that the magnetic period is double that of the chemical bilayer thickness does not require a polarized beam. However, in order to distinguish collinear from noncollinear structures and to obtain other information about moment orientation, it is necessary to use a polarized incident beam and analyze the polarization of the reflected beam, as has been discussed in preceding sections. For example, a PNR investigation of a Co/Cu(1 1 1) superlattice by Schreyer et al. [68] revealed a new in-plane anisotropy. Figs. 10 and 11 show the PNR data and scattering length density profiles with magnetization direction, respectively, for this Co/Cu(1 1 1) system as determined from a nonlinear least-squares fit using the dynamical theory outlined in Table 1. Table 3 lists the fitted parameter values. Because of the in-plane anisotropy, the magnetization direction in the Co layers could be rotated from the vertical neutron polarization axis (defined by a small applied field of about 14 G), in this case by 30° (or 60° from the horizontal). Another PNR study of Fe/Cr(1 0 0) superlattices by Schreyer et al. [69] has confirmed a noncollinear alignment of ferromagnetic Fe blocks across the Cr layers which gives credence to the predictions of a biquadratic exchange coupling. A review of this work is presented by Schreyer at this Conference [70].

Table 3
Fitted parameters from SPNR data

l	Type	Re(Nb) (10^{-6} Å^{-2})	d_b (Å)	σ_b (Å)	Re(Np) (10^{-6} Å^{-2})	d_p (Å)	σ_p (Å)	θ (deg)
1	CuO_x	3.3	45.0	5.8	0	45.0	5.8	0
2, 4, ..., 12	Co	2.0	41.1 ± 3.3	7.1	3.6	41.1 ± 3.3	7.1	60
3, 5, ..., 11	Cu	5.6	18.6 ± 1.2	7.1	0	18.6 ± 1.2	7.1	0
13	Al_2O_3	5.2	...	2.1	0	...	2.1	0

From left to right these are: layer number l (layer 0 is incident air); a brief description of the layer; real part of the average nuclear scattering density Re(Nb); nuclear layer thickness d_b; nuclear Gaussian mixing σ_b; magnetic scattering density Re(Np); magnetic layer thickness d_p; magnetic Gaussian mixing σ_p; and the angle of the magnetic moment with respect to the spin-flip (incident beam) direction.

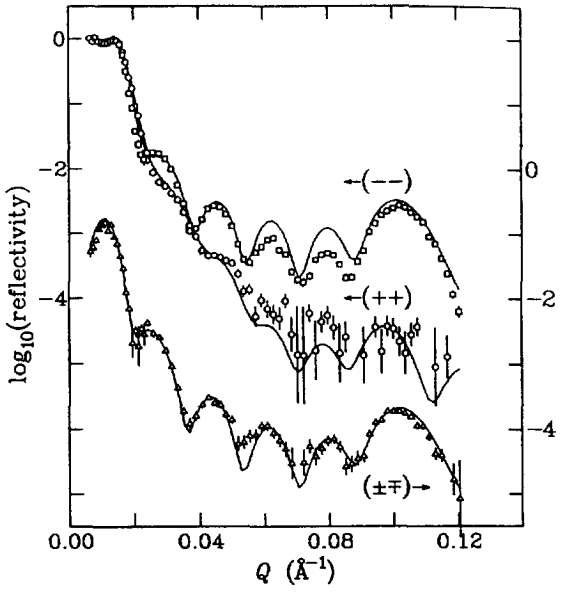

Fig. 10. PNR data for a Co/Cu(1 1 1) superlattice with a dynamical fit for the scattering length density profiles shown in Fig. 11. The SF reflectivities have been combined and are shifted downwards by two orders of magnitude. (After Ref. [68].)

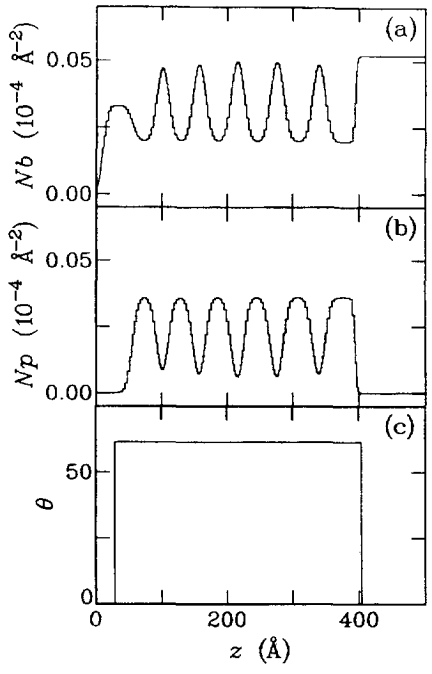

Fig. 11. Nuclear (a) and magnetic (b) scattering length density profiles corresponding to the fit of the PNR data shown in Fig. 10 for the Co/Cu(1 1 1) superlattice. The magnetization is at a constant angle relative to the neutron polarization axis as described in the text. (After Ref. [68].)

4.3. *Magnetic semiconductor and insulator superlattices*

Neutron diffraction studies of antiferromagnetic semiconductor superlattices have been reviewed by Giebultowicz et al. [71]. The effects of strain and finite size on the magnetic ordering have been studied in a number of different systems including MnSe/ZnTe and MnSe/ZnSe. In MnTe/CdTe systems with very thin nonmagnetic CdTe spacer layers, interlayer coupling has been observed. Neutron diffraction studies of EuTe/PbTe(111) superlattices have shown that the antiferromagnetic EuTe layers couple across large thicknesses of the nonmagnetic PbTe spacers (up to 55 Å) despite the relatively low carrier concentration and consequential improbability of an RKKY interaction [72].

Neutron diffraction measurements have also revealed the propagation of the antiferromagnetic spin order in NiO layers through ostensibly paramagnetic and insulating layers of CoO in a (111)NiO/CoO superlattice system [73].

4.4. *Ultrathin ferromagnetic films*

How the magnetic moments of a ferromagnetic material at the surface or at an interface with another material are affected is a problem of fundamental physical interest.

The thickness of the magnetic layer, its crystallographic orientation, the epitaxial strain created by a given substrate, and the electronic structure of the substrate all influence, to some degree, the ultimate magnetic state of the deposited film. Theoretical predictions based on ab initio calculations have been made for numerous thin film systems [74, 75]. A variety of techniques, including spin-polarized photo-emmission, the magneto-optic Kerr effect, spin-polarized low-energy electron diffraction, Mossbauer spectroscopy, ferromagnetic resonance, and superconducting quantum interference device magnetometry, have been applied, in addition to PNR, to the study of ultrathin film magnetism (see, for example, the review by Falicov et al. [75]). Although the determination of the absolute magnetic moment per atom in an ultrathin film is extremely challenging for whatever technique or combination thereof is used, PNR offers some notable advantages; namely, straightforward quantitative analysis of the data and relatively high sensitivity to the ferromagnetic film compared to a possible diamagnetic response from a substrate of much greater volume. Felcher et al. [76] showed that certain overlayers could be used to further enhance the sensitivity of PNR to the thin ferromagnetic layer. A discussion of the quantitative accuracy to which the magnitude of the moment in ultrathin films can be obtained by PNR measurements is given in a review by Felcher [77].

The first ultrathin magnetic films studied by PNR were metastable FCC Co and FCC Fe on Cu(0 0 1) by Bland et al. [78]. It was reported that the Co moment was close to that in the bulk whereas an in-plane ferromagnetic Fe moment was absent, in marked contrast to a BCC Fe film of comparable thickness. Subsequent PNR studies on various Co thin-film sandwiches have been carried out [79–81]. A systematic PNR study of BCC Fe films of various thicknesses (as low as 4 Å) on MgO and capped with Au has also been performed [82]. A dramatic decrease in the Curie temperature and a magnetization axis tilted out of the film surface were observed for the thinnest Fe films. However, at 40 K all of the films were found to be ferromagnetic with an average moment per Fe ion equal to 2.2 ± 0.2 Bohr magnetons regardless of film thickness [82]. More recently, Bland et al. [83] have reported enhanced magnetic moments in epitaxial Fe films grown on Ag(0 0 1) substrates with various overlayers using both PNR and ferromagnetic resonance techniques. Particular consideration was given to the effects of roughness and the treatment of diffuse scattering. For instance, for approximately 5 monolayers of (0 0 1) Fe sandwiched between the Ag substrate and Ag and Au overlayers, a layer-averaged moment per Fe atom of 2.58 ± 0.09 Bohr magnetons was deduced from the PNR measurements, compared to a bulk value of 2.22.

5. Future directions

In addition to continuing and expanding the types of polarized neutron scattering studies described in the preceding sections, other kinds of measurements with polarized neutrons are feasible which could contribute to a better understanding of magnetism in thin films and superlattices. In this section, two specific possibilities will be discussed.

The first has to do with the measurement of nonspecular or diffuse scattering. In contrast to specular scattering, with which nearly all of the work described above has exclusively dealt, nonspecular scattering can provide information about in-plane inhomogeneities in the magnetic structure, particularly as might occur at an interface. The roughness of buried interfaces is considered to be one of the most difficult properties of magnetic thin films and superlattices to either characterize or control [84] and is suspected to significantly affect the behavior of GMR superlattices. A considerable amount of work has been done on the problem of nonspecular scattering by X-rays and specific studies of diffuse neutron scattering from magnetic interfaces, though not yet nearly as extensive, have also been performed. General discussions of the diffuse scattering of neutrons from magnetic interfaces have been given by Felcher [77, 85], Sinha [86], and Syromyatnikov et al. [87]. One of the most interesting measurements of nonspecular neutron scattering was performed by Takeda et al. [88, 89] on Fe/Cr superlattices. Recall, from the discussions of these GMR superlattices above, that in the case of antiparallel alignment of the ferromagnetic Fe blocks across the intervening Cr, a superlattice satellite peak appears about the forward direction at a value of Q which corresponds to twice the chemical bilayer thickness of the Fe and Cr layers. Takeda et al. measured the diffuse neutron scattering in two transverse scans perpendicular to the longitudinal axis which is parallel to the growth direction. One of these scans intercepted the longitudinal axis at the value of Q associated with the antiparallel satellite position while the other crossed at the chemical period position. Ridges of diffuse scattering were observed at both of these locations, each peaking at the respective specular position on the longitudinal axis. However, the diffuse scattering through the antiparallel superlattice peak position was found to be stongly suppressed with applied magnetic field whereas that through the chemical peak position was enhanced. The diffuse scattering about the antiparallel specular peak position must therefore be due to a magnetic "roughness". Takeda et al. also found that the magnitude of this magnetic diffuse scattering is correlated with the size of the GMR effect [88, 89]. Further analysis of these results, including the effect of conformal roughness, is discussed by Sinha [86]. In another study of the off-specular scattering of neutrons by Fe/Cr superlattices, Hahn et al. [90] concluded that although the magnetic domains are laterally limited, their size is not directly correlated to the magnetoresistance,

i.e., that the GMR effect in Fe/Cr superlattices is not directly dependent on the number of magnetic domain boundaries. Their conclusion supports the hypothesis that the origin of the magnetoresistance is connected with interfacial roughness or imperfections. Magnetic diffuse neutron scattering has already contributed to the understanding of GMR systems and has the potential to provide more quantitative detail regarding the magnetic structure of the interface.

A second possible direction for neutron scattering in the investigation of magnetic superlattices pertains to the role of the nonferromagnetic spacer in superlattices with coupled magnetic layers. It would be very interesting to see whether, for example, a spin density wave exists in the intervening Y layer between magnetic layers such as Dy. However, because the magnetic scattering of neutrons is proportional to the square of the atomic magnetic moment, sensitivity is limited by moment magnitude. Presumably, a spin density wave in Y would have an effective moment per atom that is only a fraction of a Bohr magneton, and significantly smaller than that of Dy. On the other hand, the situation for Fe/Cr superlattices is somewhat better since the Cr moment is fractionally larger compared to Fe.

Recent work has shown that in Fe/Cr(0 0 1) superlattices: (a) Cr long-range anti-ferromagnetic order (an incommensurate spin density wave in the bulk) is suppressed for Cr layer thicknesses less than 42 Å; and (b) the biquadratic coupling of the Fe layers, observed in superlattices where the Cr does order, vanishes below the Neel temperature of the Cr layers [91, 92]. These are interesting results. Nonetheless, the antiferromagnetic order of the Cr was inferred from bulk measurements: the actual microscopic structure has not been confirmed to be that of bulk Cr. Is it possible to distinguish various magnetic configurations of the Cr moments in Fe/Cr(0 0 1) superlattices by polarized neutron diffraction methods? In principle, yes, in practice, probably. In Fig. 12 are shown several calculated PNR curves and corresponding Cr moment arrangements over a range of Q where significant differences are evident. The calculations were performed assuming the nuclear and magnetic scattering densities for Fe and Cr and using the interplanar spacings of (0 0 1) Fe and Cr. The superlattice consists of 10 Fe planes and 22 Cr planes in a chemical bilayer repeated 6 times. In all cases the ferromagnetic layers are aligned antiparallel to one another (along a vertical axis) so that the magnetic unit is twice the chemical bilayer thickness. The magnetizations of both the Fe and Cr atomic planes are taken to lie in-plane with the neutron polarization taken to be along the vertical axis. The dynamical reflectivity formulas of Table 1 have been used, the only artifice being that the scattering densities are taken to be confined, for each atomic plane, to one-fourth the interplanar (0 0 1) spacing: as discussed in Section 2, the consequences of this are to affect the intensities at these higher values of Q by only a few percent. It is clear from the reflectivity curves that a combination of SF and

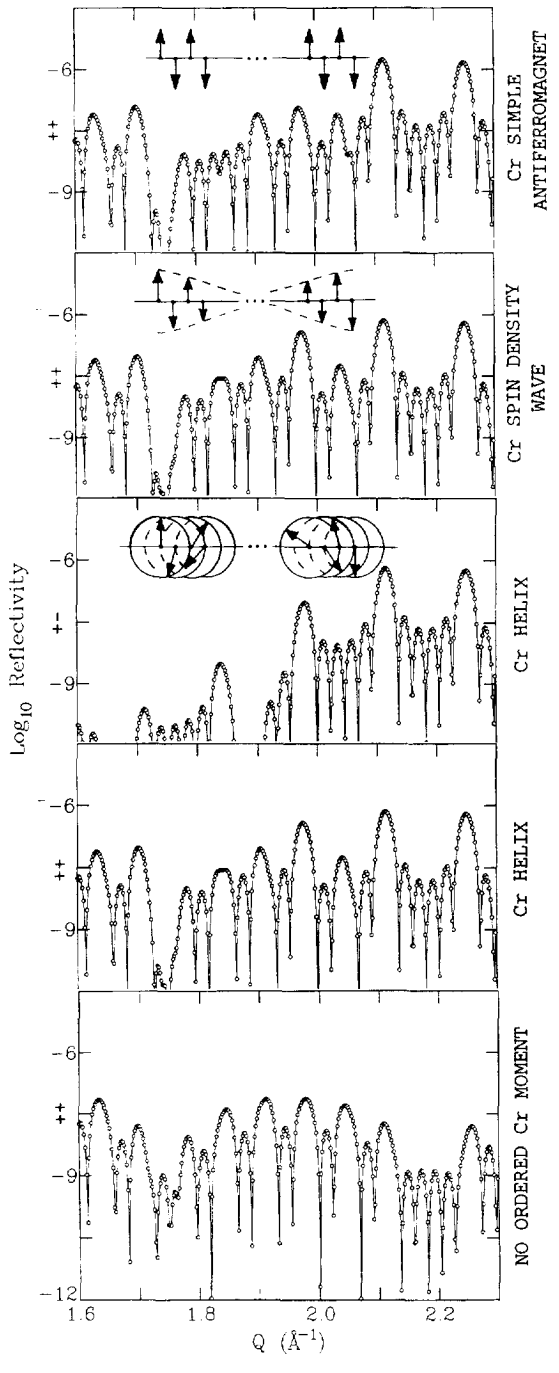

Fig. 12. Calculated PNS curves and corresponding Cr moment arrangements for the Fe/Cr(0 0 1) superlattice system described in the text. Over this range of wave vector transfer, PNS can, in principle, be used to distinguish these possible moment configurations from one another.

NSF PND data can, in principle, distinguish the simple antiferromagnetic, spin density wave, helical, and disordered Cr layer moment configurations from one another. In practice, the reflectivity magnitudes are such that a sample with a film surface area of about 10 cm^2 and perhaps 10 times as many bilayers would be enough to measure the more prominent and key features necessary to identify a particular model by PND with existing instrumentation. If successful, measurements such as these could help resolve some of the important questions regarding the interlayer coupling mechanism in magnetic superlattices.

6. Conclusion

Neutron scattering techniques have proved to be indispensable in determining the detailed microscopic arrangement of magnetic moments exhibiting long-range order in atomically engineered epitaxial thin films and superlattices. From the confirmation of antiparallel interlayer alignment to the quantitative measurement of magnetization depth profiles and absolute values of atomic magnetic moments, neutron scattering measurements, particularly PND and PNR, have made contributions of fundamental significance to the understanding of the intricate magnetic interactions manifest in layered film structures. These contributions have both corroborated and complemented the information obtained by other important but either volume-averaging or strictly surface-sensitive magnetic probes. Early scepticism of the practical application of neutron scattering to the study of samples with such exceedingly small volumes, compared to that of conventional bulk specimens, has been shown to be unfounded. Nonetheless, intensity limitations remain the principal challenge to practitioners of the method. As neutron sources improve and beam optics become more efficient, further scientific advances in the investigation of magnetic phenomena can be expected.

Acknowledgements

It is a pleasure to acknowledge the colleagues with whom I have had the privilege of working on some of the measurements described here and to thank those who sent reprints about research that they have been engaged in, namely, J. Bland, R. Cowley, G. Felcher, Y. Endoh, T. Giebultowicz, P. Mangin, J. Martinez and J. Penfold.

References

[1] G.E. Bacon, Neutron Diffraction (Oxford, London, 1975; 3rd ed.).
[2] M. Blume, Phys. Rev. 130 (1963) 1670.
[3] R.M. Moon, T. Riste and W.C. Koehler, Phys. Rev. 181 (1969) 920.
[4] M.Th. Rekveldt, J. Phys. (Paris) C1 (1971) 579.
[5] A.I. Okorokov, V.V. Runov and A.G. Gukasov, Nucl. Instr. and Meth. 157 (1978) 487.
[6] F. Tasset, P.J. Brown and J.B. Forsyth, J. Appl. Phys. 63 (1988) 3606.
[7] V. Nunez, P.J. Brown, J.B. Forsyth and F. Tasset, Physica B 174 (1991) 60.
[8] S.J. Blundell and J.A.C. Bland, Phys. Rev. B 46 (1992) 3391.
[9] N.K. Pleshanov, Z. Phys. B 94 (1994) 233.
[10] S.K. Mendiratta and M. Blume, Phys. Rev. B 14 (1976) 144.
[11] P.J. Sivardiere, Acta Crystallogr. A 31 (1975) 340.
[12] V.A. Belyakov and R.Ch. Bokun, Fiz. Tverd. Tela (Leningrad) 18 (1976) 2399 [Sov. Phys. – Solid State 18 (1976) 1399].
[13] O. Scharpf, J. Appl. Crystallogr. 11 (1978) 626.
[14] G.P. Felcher, R.O. Hilleke, R.K. Crawford, J. Haumann, R. Kleb and G. Ostrowski, Rev. Sci. Instr. 58 (1987) 609.
[15] C.F. Majkrzak, Physica B. 156 & 157 (1989) 619.
[16] C.F. Majkrzak and N.F. Berk, Phys. Rev. B 40 (1989) 371.
[17] M. Büttiker, Phys. Rev. B 27 (1983) 6178.
[18] V. Nunez, C.F. Majkrzak and N.F. Berk, MRS Symp. Proc. 313 (1993) 431.
[19] V. Nunez, N.F. Berk and C.F. Majkrzak, Bull. Am. Phys. Soc. 39 (1994) 313.
[20] V. Nunez, C.F. Majkrzak and N.F. Berk, unpublished experimental results, Reactor Radiation Division, NIST (October 1993).
[21] J.A.C. Bland, R. Bateson and G. Hird, J. Phys.: Condens. Matter 1 (1989) 4399.
[22] C.F. Majkrzak, J. Kwo, M. Hong, Y. Yafet, D. Gibbs, C.L. Chien and J. Bohr, Adv. Phys. 40 (1991) 99.
[23] C.F. Majkrzak, J.F. Ankner, N.F. Berk and D. Gibbs, in: Magnetic Multilayers, eds. L.H. Bennett and R.E. Watson (World Scientific, Singapore, 1994) p. 299.
[24] F. Mezei, Comm. Phys. 1 (1976) 81.
[25] M.Th. Rekveldt, J. Phys. (Paris) C1 (1971) 579.
[26] O. Schärpf, Physica B 156 & 157 (1989) 631.
[27] C.F. Majkrzak, V. Nunez, J.R.D. Copley, J.F. Ankner and G.C. Greene, in: Neutron Optical Devices and Applications, SPIE Proc., Vol. 1738, eds. C.F. Majkrzak and J. Wood (SPIE, Bellingham, WA, 1992) p. 90.
[28] C.F. Majkrzak, in: Handbook of Neutron Scattering, ed. W. Gläser (Springer, Berlin, in press).
[29] J.F. Ankner, A. Schreyer, Th. Zeidler, C.F. Majkrzak, H. Zabel, J.A. Wolf and P. Grunberg, MRS Symp. Proc. 313 (1993) 761.
[30] S.M. Durbin, J.E. Cunningham and C.P. Flynn, J. Phys. F 12 (1982) L75.
[31] J. Kwo, D.B. McWhan, M. Hong, E.M. Gyorgy, L.C. Feldman and J.E. Cunningham, in: Layered Structures, Epitaxy, and Interfaces, eds. J.H. Gibson and L.R. Dawson, Materials Research Society Symp. Proc., Vol. 37 (Materials Research Society, Pittsburgh, PA, 1985) p. 509.
[32] J.J. Rhyne and R.W. Erwin, in: Magnetic Materials, Vol. 8, ed. K.H.J. Buschow (North-Holland, Elsevier, Amsterdam, 1995) p. 1.
[33] C.F. Majkrzak, J.W. Cable, J. Kwo, M. Hong, D.B. McWhan, Y. Yafet, J.V. Waszczak and C. Vettier, Phys. Rev. Lett. 56 (1986) 2700.

[34] Y. Yafet, J. Kwo, M. Hong, C.F. Majkrzak and T. O'Brien, J. Appl. Phys. 63 (1988) 3453.
[35] C. Vettier, D.B. McWhan, E.M. Gyorgy, J. Kwo, B.M. Buntschuh and B.W. Batterman, Phys. Rev. Lett. 56 (1986) 757.
[36] C.F. Majkrzak, J. Cable, J. Kwo, M. Hong, D.B. McWhan, Y. Yafet, J.V. Waszczak, H. Grimm and C. Vettier, J. Appl. Phys. 61 (1987) 4055.
[37] M.B. Salamon, S. Sinha, J.J. Rhyne, J.E. Cunningham, R.W. Erwin, J. Borchers and C.P. Flynn, Phys. Rev. Lett. 56 (1986) 259.
[38] Y. Yafet, J. Appl. Phys. 61 (1987) 4058.
[39] Y. Yafet, in: Magnetic Multilayers, eds. L.H. Bennett and R.E. Watson (World Scientific, Singapore, 1994) p. 19.
[40] C.P. Flynn, F. Tsui, M.B. Salamon, R.W. Erwin and J.J. Rhyne, J. Phys.: Condens. Matter 1 (1989) 5997.
[41] R.W. Erwin, J.J. Rhyne, M.B. Salamon, J. Borchers, S. Sinha, R. Du, J.E. Cunningham and C.P. Flynn, Phys. Rev. B 35 (1987) 6808.
[42] R.S. Beach, J.A. Borchers, A. Matheny, R.W. Erwin, M.B. Salamon, B. Everitt, K. Pettit, J.J. Rhyne and C.P. Flynn, Phys. Rev. Lett. 70 (1993) 3502.
[43] D. Gibbs, D.E. Monction, K.L. D'Amico, J. Bohr and B.H. Grier, Phys. Rev. Lett. 55 (1985) 234.
[44] D. Gibbs, J. Bohr, J.D. Axe, D.E. Moncton and K.L. D'Amico, Phys. Rev. B 34 (1986) 8182.
[45] J. Bohr, D. Gibbs, D.E. Moncton and K.L. D'Amico, Physica A 140 (1986) 349.
[46] R.A. Cowley and S.J. Bates, J. Phys. C 21 (1986) 4113.
[47] J. Bohr, D. Gibbs, J.D. Axe, D.E. Moncon, K.L. D'Amico, C.F. Majkrzak, J. Kwo, M. Hong, C.L. Chien and J. Jensen, Physica B 159 (1989) 93.
[48] D.F. McMorrow, D.A. Jehan, R.A. Cowley, P.P. Swaddling, R.C.C. Ward, M.R. Wells, N. Hagmann and K.N. Claussen, Europhys. Lett. 23 (1993) 523.
[49] D.F. McMorrow, D.A. Jehan, P.P. Swaddling, R.A. Cowley, R.C.C. Ward and M.R. Wells, Physica B 192 (1993) 150.
[50] D.A. Jehan, D.F. McMorrow, R.A. Cowley, R.C.C. Ward, M.R. Wells and N. Hagmann, Phys. Rev. B 48 (1993) 5594.
[51] R.A. Cowley, D.F. McMorrow, A. Simpson, D. Jehan, P. Swaddling, R.C.C. Ward and M.R. Wells, J. Appl. Phys. 76 (1994) 6274.
[52] J.A. Simpson, D.F. McMorrow, R.A. Cowley, D.A. Jehan, R.C.C. Ward, M.R. Wells and K.N. Clausen, Phys. Rev. Lett. 73 (1994) 1162.
[53] J.A. Borchers, M.B. Salamon, R.W. Erwin, J.J. Rhyne, R.R. Du and C.P. Flynn, Phys. Rev. B 43 (1991) 3123.
[54] P.M. Gehring, K. Hirota, C.F. Majkrzak and G. Shirane, Phys. Rev. Lett. 71 (1993) 1087.
[55] K. Hirota, G. Shirane, P.M. Gehring and C.F. Majkrzak, Phys. Rev. B 49 (1994) 11 967.
[56] P.M. Gehring, K. Hirota, C.F. Majkrzak and G. Shirane, Phys. Rev. B 51 (1995) 3234.
[57] T.R. Thurston, G. Helgesen, D. Gibbs, J.P. Hill, B.D. Gaulin and G. Shirane, Phys. Rev. Lett. 70 (1993) 3151.
[58] P. Gehring et al., Physica B 221 (1996) 398.
[59] L.M. Falicov, Physics Today 46 (1992).
[60] A. Cebollada, J.L. Martinez, J.M. Gallego, J.J. deMiguel, R. Miranda, S. Ferrer, F. Battalan, G. Fillion and J.P. Rebouillat, Phys. Rev. B 39 (1989) 9726.
[61] A. Barthélémy, A. Fert, M.N. Baibich, S. Hadjoudj, F. Petroff, P. Etienne, R. Cabanel, R. Lequien, F. Nguyen van Dau and G. Creuzet, J. Appl. Phys. 67 (1990) 5908.
[62] H. Hosoito, S. Araki, K. Mibo and T. Shinjo, J. Phys. Soc. Japan 59 (1990) 1925.
[63] W. Schwarzacher, W. Allison, J. Penfold, C. Shackleton, C.D. England, W.R. Bennet, J.R. Dutcher and C.M. Falco, J. Appl. Phys. 69 (1991) 4040.
[64] S.S.P. Parkin, A. Mansour and G.P. Felcher, Appl. Phys. Lett. 58 (1991) 1473.
[65] J.L. Martiniz, Physica B 180 & 181 (1992) 39.
[66] N. Hosoito, K. Mibu, S. Araki, T. Shinjo, S. Itoh and Y. Endoh, J. Phys. Soc. Japan 61 (1992) 300.
[67] J.A.C. Bland, R.D. Bateson, N.F. Johnson, S.J. Blundell, V.S. Speriosu, S. Metin, B.A. Gurney and J. Penfold, J. Magn. Magn. Mater. 123 (1993) 320.
[68] A. Schreyer, Th. Zeidler, Ch. Morawe, N. Metoki, H. Zable, J.F. Ankner and C.F. Majkrzak, J. Appl. Phys. 73 (1993) 7616.
[69] A. Schreyer, J.F. Ankner, H. Zable, M. Schäfer, C.F. Majkrzak and P. Grünberg, Physica B 198 (1994) 173.
[70] A. Schreyer et al., Physica B 221 (1996) 366.
[71] T.M. Giebultowicz, H. Luo, N. Samarth, J.K. Furdyna, V. Nunez, J.J. Rhyne, W. Faschinger, G. Springholtz, G. Bauer and H. Sitter, Physica B 198 (1994) 163.
[72] T.M. Giebultowicz, V. Nunez, G. Springholz, G. Bauer, J. Chen, M.S. Dresselhaus and J.K. Furdyna, J. Magn. Magn. Mater. 140–144, (1995), in press.
[73] J.A. Borchers, M.J. Carey, R.W. Erwin, C.F. Majkrzak and A.E. Berkowitz, Phys. Rev. Lett. 70 (1993) 1878.
[74] C.L. Fu, A.J. Freeman and T. Oguchi, Phys. Rev. Lett. 54 (1985) 2700.
[75] L.M. Falicov, D.T. Pierce et al., J. Mater. Res. 5 (1990) 1299.
[76] G.P. Felcher, K.E. Gray, R.T. Kampwirth and M.B. Brodsky, Physica B 136 (1986) 59.
[77] G.P. Felcher, Phys. B 192 (1993) 137.
[78] J.A.C. Bland, D. Pescia and R.F. Willis, Phys. Rev. Lett. 58 (1987) 1244.
[79] J.A.C. Bland, R.D. Bateson, P.C. Ried, R.G. Graham, H.J. Lauter, J. Penfold and C. Shackleton, J. Appl. Phys. 69 (1991) 4989.
[80] J.A.C. Bland, A.D. Johnson, R.D. Bateson and H.J. Lauter, J. Magn. Magn. Mater. 104–107 (1992) 1798.
[81] V.V. Pasyuk, H.J. Lauter, M.T. Johnson, F.J.A. den Broeder, E. Janssen, J.A.C. Bland and A.V. Petrenko, Appl. Surf. Sci. 65/66 (1993) 118.
[82] Y.Y. Huang, C. Liu and G.P. Felcher, Phys. Rev. B 47 (1993) 183.
[83] J.A.C. Bland, C. Daboo, B. Heinrich, Z. Celinski and R.D. Bateson, Phys. Rev. B 51 (1995) 258.
[84] G.A. Prinz, Phys. Today 48 (1995) 58.
[85] G.P. Felcher, Physica B 198 (1994) 150.
[86] S.K. Sinha, MRS Symp. Proc. 376 (1995), in press.
[87] V. Syromyatnikov, B. Toperverg, A. Schebetov, T. Ebel, C. Bittorf, R. Kampmann and R. Wagner, Effect of coherent enhancement of nonspecular polarized neutron scattering from rough interfaces in periodic multilayered magnetic structures, Preprint 2006, Russian Academy of Sciences, Petersburg, Nuclear Physics Institute.
[88] M. Takeda, Y. Endoh, H. Yasuda, K. Yamada, A. Kamijo and J. Mizuki, J. Phys. Soc. Japan 62 (1993) 3015.

[89] Y. Endoh, M. Takeda, A. Kamijo, J. Mizuki, N. Hosoito and T. Shinjo, Mater. Sci. Eng. B, in press.
[90] W. Hahn, M. Loewenhaupt, G.P. Felcher, Y.Y. Huang and S.S.P. Parkin, J. Appl. Phys. 75 (1994) 3564.
[91] E.E. Fullerton, K.T. Riggs, C.H. Sowers, S.D. Bader and A. Berger, Phys. Rev. Lett., submitted.
[92] S. Adenwalla, G.P. Felcher, E.E. Fullerton and S.D. Bader, Phys. Rev. B, submitted.